Hindawi Publishing Corporation
EURASIP Journal on Wireless Communications and Networking
Volume 2010, Article ID 387625, 15 pages
doi:10.1155/2010/387625

Research Article

Probabilistic Coexistence and Throughput of Cognitive Dual-Polarized Networks

J.-M. Dricot,[1] G. Ferrari,[2] A. Panahandeh,[1] Fr. Horlin,[1] and Ph. De Doncker[1]

[1] *OPERA Department, Wireless Communications Group, Université Libre de Bruxelles, Belgium*
[2] *WASN Lab, Department of Information Engineering, University of Parma, Italy*

Correspondence should be addressed to J.-M. Dricot, jdricot@ulb.ac.be

Received 30 October 2009; Revised 8 February 2010; Accepted 25 April 2010

Academic Editor: Zhi Tian

Diversity techniques for cognitive radio networks are important since they enable the primary and secondary terminals to efficiently share the spectral resources in the same location simultaneously. In this paper, we investigate a simple, yet powerful, diversity scheme by exploiting the polarimetric dimension. More precisely, we evaluate a scenario where the cognitive terminals use cross-polarized communications with respect to the primary users. Our approach is network-centric, that is, the performance of the proposed dual-polarized system is investigated in terms of link throughput in the primary and the secondary networks. In order to carry out this analysis, we impose a probabilistic coexistence constraint derived from an information-theoretic approach, that is, we enforce a guaranteed capacity for a primary terminal for a high fraction of time. Improvements brought about by the use of our scheme are demonstrated analytically and through simulations. In particular, the main simulation parameters are extracted from a measurement campaign dedicated to the characterization of indoor-to-indoor and outdoor-to-indoor polarization behaviors. Our results suggest that the polarimetric dimension represents a remarkable opportunity, yet easily implementable, in the context of cognitive radio networks.

1. Introduction

Cognitive radio networks and, more generally, dynamic spectrum access networks are becoming a reality. These systems consist of primary nodes, which have guaranteed priority access to spectrum resources, and secondary (or cognitive) nodes, which can reuse the medium in an opportunistic manner [1–4]. Cognitive nodes are allowed to dynamically operate the secondary spectrum, provided that they do not degrade the primary users' transmissions [5]. From a practical viewpoint, this means that the secondary terminals must acquire a sufficient level of knowledge about the status of the primary network. This information can be gathered through the use of techniques such as energy detection [6], cyclostationary feature detection [7], and/or cooperative distributed detection [8]. Due to the complexity and drawbacks of the detection phase, the FCC recently issued the statement that all devices "must include a geolocation capability and provisions to access over the Internet a database of protected radio services and the locations and channels that may be used by the unlicensed devices at each location" [9]. Furthermore, the positions of the primary nodes and other meta-information can be shared in the same way. Though the locations of the nodes and their configurations can be obtained easily, the exploitation of such information remains an open problem. Considering that any diversity technique can be used by cognitive nodes, several approaches have been proposed to allow for the coexistence of primary and secondary networks [10]. These include, for example, the use of orthogonal codes (code division multiple access, CDMA) [11], frequency multiplexing (frequency division multiple access, FDMA), directional antennas (spatial division medium access, SDMA) [12], orthogonal frequency-division multiple access (OFDMA) [13], and time division multiple access (TDMA) [14], among others.

In this paper, we investigate a simple, yet powerful, diversity scheme by exploiting the polarimetric dimension [15–17]. More specifically, a dual-polarized wireless channel enables the use of two distinct polarization modes, referred to as *copolar* (symbol: $\parallel$) and *cross-polar* (symbol: $\perp$),

respectively. Ideally, cross-polar transmissions (i.e., from a transmitting antenna on one channel to the receiving antenna on the corresponding orthogonal channel) should be impossible. In reality, this is not the case due to an imperfect antenna cross-polar isolation (XPI) and a depolarization mechanism that occurs as electromagnetic waves propagate (i.e., a signal sent on a given polarization "leaks" into the other). Both effects combine to yield a global phenomenon referred to as cross-polar discrimination (XPD) [18–20].

The scenario of interest for this work is shown in Figure 1. The primary system consists of a single transmitter located at a distance of d_0 from its intended receiver. Without any loss of generality, the primary receiver is considered to be located at the origin of the coordinates system, leading to a *receiver-centric* analysis. The secondary (cognitive) terminals are deployed along with the primary ones. However, limitations on interference prevent them from entering a protected region around the receiver. This region, referred to as the "primary exclusive region" [21], is assumed to be circular and therefore, is completely characterized by its radius, denoted as d_{excl}.

Since polarimetric diversity does not allow a perfect orthogonality between primary and secondary nodes' transmissions, its use is possible under the application of a so-called *underlay paradigm* [10, 22, 23]. This means that both cognitive and primary terminals carry out communications, provided that the capacity loss caused by cognitive users does not degrade communication quality for primary users. For this purpose, we can further characterize the underlaid paradigm by requiring that the primary system must be guaranteed a minimum (transmission) capacity during a large fraction of time. As will be shown, this can, in turn, be formulated as a probabilistic coexistence problem under the constraint of a limited outage probability in the primary network.

We argue that using the polarimetric dimension allows dynamic spectrum sharing to be efficiently implemented in cognitive systems. To this end, we propose a theoretical model of interference in dual-polarized networks and derive a closed-form expression for the link probability of outage. We theoretically prove that polarimetric diversity can increase transmission rates for the secondary terminals while, at the same time, can significantly reduce the primary exclusive region.

First, we validated the expected (theoretical) performance gains analytically. To the best of our knowledge, none of the past studies in literature has investigated the behavior of the XPD under a complete range of propagation conditions, such as indoor-to-indoor and outdoor-to-indoor. In particular, we conducted a vast experimental campaign to provide relevant insights on the proper models and statistical distributions which would accurately represent the XPD. Based on these measures, the achievable performance of these dual-polarized cognitive networks, considering both half-duplex and full-duplex communications, will be determined.

The medium access control (MAC) protocol considered is a variant of the slotted ALOHA protocol [24] such that in each time slot, the nodes transmit independently with a certain fixed probability [25]. This approach is supported by the observations in [26, page 278] and [25, 27], where it is shown that the traffic generated by nodes using a slotted random access MAC protocol can be modeled by means of a Bernoulli distribution. In fact, in more sophisticated MAC schemes, the probability of transmission of a terminal's transmission can be modeled as a function of general parameters, such as, queuing statistics, the queue-dropping rate, and the channel outage probability incurred by fading [28]. Since the impact of these parameters is not the focus of the this study, for more details we refer the interested reader to the existing studies in the literature [29–31].

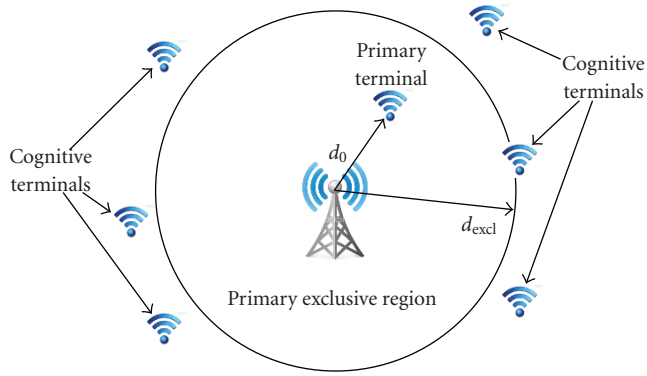

Figure 1: Cognitive network model: a single primary transmitter is placed at the center of a primary exclusive region (PER), with radius d_{excl}, where its intended receiver is present.

The remainder of this paper is organized as follows. In Section 2, we demonstrate how the polarimetric dimension increases spectrum-utilization efficiency and supports the coexistence of primary and secondary users in a probabilistic sense, which requires guaranteed capacity for the primary network. After these theoretical developments, several insights are presented to move from the concept to practical implementation. First, Section 3 presents an experimental determination of the main parameters used to characterize cognitive dual-polarized networks in indoor-to-indoor and outdoor-to-indoor situations. These results are then used in Section 4 for analytical performance evaluation. Section 5 concludes the paper.

2. The Dual-Polarized Cognitive Network Architecture

2.1. Probabilistic Coexistence and Interference. Consider the cognitive network shown in Figure 1 with two types of users: primary and secondary (cognitive). The primary network is supposed to be copolar and the cognitive network is cross-polar. Without cognitive users, the primary network would operate with background noise and with the usual interference generated by the other primary users. Let $\mathbf{C}_{\text{p}}$ (dimension: [bit/s/Hz]) be the desired capacity for a user in the primary network (In this manuscript, bold letters refer to random variables). We impose that the secondary network

operates under the following outage constraint on a primary user:

$$\mathbb{P}\left\{\mathbf{C}_{\mathrm{p}} \leq C\right\} \leq \varepsilon, \tag{1}$$

where $0 < \varepsilon < 1$ and C (dimension: [bit/s/Hz]) is a minimum per-primary user capacity. Equivalently, this constraint guarantees a primary user a maximum transmission rate of at least C for at least a fraction $(1-\varepsilon)$ of the time. Under the simplifying assumption of Gaussian signaling (Note that this assumption is expedient for analytical purposes. However, in the following the analytical predictions will be confirmed by experimental results.), the rate of this primary user can be written as a function of the signal-to-noise and interference ratio (SINR) as follows:

$$\mathbf{C}_{\mathrm{p}} = \log_2(1 + \mathbf{SINR}). \tag{2}$$

Using (2) into (1) yields

$$\begin{aligned}\mathbb{P}\left\{\mathbf{C}_{\mathrm{p}} \leq C\right\} \leq \varepsilon &\Longleftrightarrow \mathbb{P}\left\{\log_2(1+\mathbf{SINR}) \leq C\right\} \leq \varepsilon \\ &\Longleftrightarrow \mathbb{P}\left\{\mathbf{SINR} \leq 2^C - 1\right\} \leq \varepsilon\end{aligned} \tag{3}$$

and, by introducing $\theta \triangleq 2^C - 1$, one has

$$\mathbb{P}\left\{\mathbf{C}_{\mathrm{p}} \leq C\right\} \leq \varepsilon \Longleftrightarrow \mathbb{P}\{\mathbf{SINR} > \theta\} > 1 - \varepsilon, \tag{4}$$

where $\mathbb{P}\{\mathbf{SINR} > \theta\}$ can be interpreted as the primary link probability of successful transmission for an outage SINR value θ. This value depends on the receiver's characteristics, modulation, and coding scheme, among others [32]. The SINR at the end of a primary link with length d_0 can be written as

$$\mathbf{SINR} \triangleq \frac{\mathbf{P}_0(d_0)}{N_0 \mathrm{B} + \mathbf{P}_{\mathrm{int}}}, \tag{5}$$

where $\mathbf{P}_0(d_0)$ is the instantaneous received power (dimension: [W]) at distance d_0, $N_0/2$ is the noise power spectral density of the noise (dimension: [W/Hz]), B is the channel bandwidth, and $\mathbf{P}_{\mathrm{int}}$ is the cumulated interference power (dimension: [W]) at the receiver, that is, the sum of the received powers from all the undesired transmitters. We now provide the reader with a series of theoretical results, which stem from the following theorem.

Theorem 1. *In a narrowband Rayleigh block-faded dual-polarized network, where nodes transmit with probability q on the copolar and the cross-polar channels, the probability that the SINR exceeds a given value θ on a primary transmission, given a fixed transmitter-receiver distance d_0, $N_{\mathrm{int}}^{\parallel}$ copolar interferers at distances $\{d_i\}_{i=1}^{N_{\mathrm{int}}^{\parallel}}$ transmitting at powers $\{P_i^{\parallel}\}_{i=1}^{N_{\mathrm{int}}^{\parallel}}$, and $N_{\mathrm{int}}^{\perp}$ cross-polar interferers at distances $\{d'_j\}_{j=1}^{N_{\mathrm{int}}^{\perp}}$ transmitting at powers $\{P_j^{\perp}\}_{j=1}^{N_{\mathrm{int}}^{\perp}}$ with a cross-polar discrimination coefficient XPD_0, is*

$$\begin{aligned}&\mathbb{P}\{\mathbf{SINR} > \theta\} \\ &= \exp\left(-\theta \frac{N_0 B}{P_0 d_0^{-\alpha}}\right) \times \prod_{i=1}^{N_{\mathrm{int}}^{\parallel}} \left\{1 - \frac{\theta q}{\left(P_0/P_i^{\parallel}\right)(d_i/d_0)^{\alpha} + \theta}\right\} \\ &\quad \times \prod_{j=1}^{N_{\mathrm{int}}^{\perp}} \left\{1 - \frac{\theta q}{\mathrm{XPD}_0 G(d, d_{\mathrm{ref}})\left(P_0/P_j^{\perp}\right)\left(d'_j/d_0\right)^{\alpha} + \theta}\right\},\end{aligned} \tag{6}$$

where P_0 is the transmit power, N_0B is the average power of the background noise, θ is the SINR threshold, α is the path loss exponent, XPD_0 is the reference cross-polar discrimination of the antenna at a reference distance d_{ref}, and $G(d, d_{\mathrm{ref}})$ is a function that characterizes the polarization loss over distance.

Proof. We assume a narrowband Rayleigh block fading propagation channel. The instantaneous received power $\mathbf{P}(d)$ from a node is exponentially distributed [33] with temporal-average received power $\mathbb{E}_t[\mathbf{P}(d)] = P(d) = P \cdot L(d)$, where P denotes the transmit power and $L(d) \propto d^{-\alpha}$ is the path loss at distance d (it accounts for the antenna gains and carrier frequency). The received power is then a random variable with the following probability density function:

$$f_{\mathbf{P}}(x) = \frac{1}{P(d)} \exp\left\{-\frac{x}{P(d)}\right\} = \frac{1}{P \cdot L(d)} \exp\left\{-\frac{x}{P \cdot L(d)}\right\}. \tag{7}$$

In a dual-polarized system, the cross-polar discrimination (XPD) is defined as the ratio of the temporal-average power emitted on the cross-polar channel and the temporal-average power received in the copolar channel [15], that is,

$$P^{(\perp \to \parallel)}(d) = \frac{P^{\perp}(d)}{\mathrm{XPD}(d)}, \tag{8}$$

where d is the transmission distance, $P_j^{(\perp \to \parallel)}(d) \triangleq \mathbb{E}_t[\mathbf{P}^{(\perp \to \parallel)}(d)]$ is the temporal-average value of the instantaneous leaked power $\mathbf{P}^{(\perp \to \parallel)}(d)$, and $P^{\perp}(d) \triangleq \mathbb{E}_t[\mathbf{P}^{\perp}(d)]$ is the temporal-average value of the instantaneous cross-polar power $\mathbf{P}^{\perp}(d)$. In a generic situation, the XPD is subject to spatial variability [19] and, therefore, in the context of this network-level analysis, we define the XPD in a spatial-average sense, that is,

$$\mathrm{XPD}(d) \triangleq \left\langle \frac{P^{\perp}(d)}{P^{(\perp \to \parallel)}(d)} \right\rangle, \tag{9}$$

where the operator $\langle X \rangle$ denotes the average of the value X computed on multiple different locations at the same distance d. Note that, even though the XPD is considered here in a spatial-average sense, it is possible to accommodate its expected variability for the purpose of ensuring a required minimum cross-polar discrimination. This will be detailed

in Section 4. Finally, it is shown in [17–19], that XPD(d), defined according to (9), can be expressed as follows:

$$\mathrm{XPD}(d) = \mathrm{XPD}_0 G(d, d_{\mathrm{ref}}), \tag{10}$$

where $\mathrm{XPD}_0 \geq 1$ is the XPD value at a reference distance d_{ref} and the function $G(d, d_{\mathrm{ref}}) \leq 1$ characterizes the depolarization experienced over the distance.

Let the traffic at the $N_{\mathrm{int}}^{\parallel}$ primary and $N_{\mathrm{int}}^{\perp}$ cognitive interfering nodes be modeled through the use of independent indicators $\{\Lambda_i\}_{i=1}^{N_{\mathrm{int}}^{\parallel}}$, $\{\Lambda'_j\}_{j=1}^{N_{\mathrm{int}}^{\perp}}$, with for all $i, j; \Lambda_i, \Lambda'_j \in \{0, 1\}$. In other words, $\{\Lambda_i\}$ and $\{\Lambda'_j\}$ are sequences of independent and identically distributed (iid) Bernoulli random variables: if, in a given time slot, one of these indicators is equal to 1, then the corresponding node is transmitting; if, on the other hand, the indicator is equal to 0, then the node is not transmitting. We also assume that the traffic distribution is the same at all interfering nodes of the network, that is, for all $i, \mathbb{P}\{\Lambda_i = 1\} = q$ and for all $j, \mathbb{P}\{\Lambda'_j = 1\} = q$, which is supported by the analyses presented in [25, 27, 34]. The overall interference power at the receiver is the sum of the interference powers due to copolarized and cross-polarized (leaked because of depolarization) interference powers, that is,

$$\mathbf{P}_{\mathrm{int}} = \sum_{i=1}^{N_{\mathrm{int}}^{\parallel}} \mathbf{P}_i^{\parallel}(d_i)\Lambda_i + \sum_{j=1}^{N_{\mathrm{int}}^{\perp}} \mathbf{P}_j^{(\perp\to\parallel)}\left(d_j\right)\Lambda'_j, \tag{11}$$

where $\{\mathbf{P}_i^{\parallel}(d_i)\}$ and $\{\mathbf{P}_j^{(\perp\to\parallel)}(d_j)\}$ are the (instantaneous) interfering powers at the receiver. The probability that the SINR at the receiver exceeds θ can thus be expressed as follows:

$$\begin{aligned}
&\mathbb{P}\{\mathbf{SINR} > \theta\} \\
&= \mathbb{E}_{\mathbf{P}_{\mathrm{int}}}[\mathbb{P}\{\mathbf{SINR} > \theta\} \mid \mathbf{P}_{\mathrm{int}}] \\
&= \mathbb{E}_{\{\mathbf{P}_i^{\parallel}\},\{\Lambda_i\},\{\mathbf{P}_j^{(\perp\to\parallel)}\},\{\Lambda'_j\}} \\
&\quad \times \left[\exp\left(-\frac{\theta}{P_0 L(d_0)} \times \left(N_0 B + \sum_{i=1}^{N_{\mathrm{int}}^{\parallel}} \mathbf{P}_i^{\parallel}(d_i)\Lambda_i + \sum_{j=1}^{N_{\mathrm{int}}^{\perp}} \mathbf{P}_j^{(\perp\to\parallel)}\left(d_j\right)\Lambda'_j\right)\right)\right] \\
&= \exp\left(-\theta\frac{N_0 B}{P_0 L(d_0)}\right) \\
&\quad \times \mathbb{E}_{\{\mathbf{P}_i^{\parallel}\},\{\Lambda_i\},\{\mathbf{P}_j^{(\perp\to\parallel)}\},\{\Lambda'_j\}} \\
&\quad \times \left[\prod_{i=1}^{N_{\mathrm{int}}^{\parallel}} \exp\left(-\frac{\theta \mathbf{P}_i{}^{\parallel}(d_i)\Lambda_i}{P_0 L(d_0)}\right) \times \prod_{j=1}^{N_{\mathrm{int}}^{\perp}} \exp\left(-\frac{\theta \mathbf{P}_j^{(\perp\to\parallel)}\left(d_j\right)\Lambda'_j}{P_0 L(d_0)}\right)\right],
\end{aligned} \tag{12}$$

where in the second passage, we have exploited the fact that, in a Rayleigh faded transmission, the SINR is also exponentially-distributed [33]. Since all terminals have an independent transmission behavior and are subject to noncorrelated channel fading, that is, $\{\mathbf{P}_i^{\parallel}\}, \{\Lambda_i\}, \{\mathbf{P}_j^{(\perp\to\parallel)}\}$, and $\{\Lambda'_j\}$ are independent sets of random variables, it then holds that

$$\begin{aligned}
&\mathbb{P}\{\mathbf{SINR} > \theta\} \\
&\quad = \exp\left(-\theta\frac{N_0 B}{P_0 L(d_0)}\right) \\
&\qquad \times \prod_{i=1}^{N_{\mathrm{int}}^{\parallel}} \mathbb{E}_{\{\mathbf{P}_i^{\parallel}\},\{\Lambda_i\}}\left[\exp\left(-\frac{\theta \mathbf{P}_i^{\parallel}(d_i)\Lambda_i}{P_0 L(d_0)}\right)\right] \\
&\qquad \times \prod_{j=1}^{N_{\mathrm{int}}^{\perp}} \mathbb{E}_{\{\mathbf{P}_j^{(\perp\to\parallel)}\},\{\Lambda'_j\}}\left[\exp\left(-\frac{\theta \mathbf{P}_j^{(\perp\to\parallel)}\left(d_j\right)\Lambda'_j}{P_0 L(d_0)}\right)\right].
\end{aligned} \tag{13}$$

The generic first expectation term at the right-hand side of (13) can be expressed as follows:

$$\begin{aligned}
&\mathbb{E}_{\{\mathbf{P}_i^{\parallel}\},\{\Lambda_i\}}\left[\exp\left(-\frac{\theta \mathbf{P}_i^{\parallel}(d_i)\Lambda_i}{P_0 L(d_0)}\right)\right] \\
&\quad = \mathbb{P}\{\Lambda_i = 1\} \times \int_0^{\infty} \exp\left(-\frac{\theta p_i}{P_0 L(d_0)}\right) f_{\mathbf{P}_i^{\parallel}}(p_i)\,\mathrm{d}p_i \\
&\qquad + \mathbb{P}\{\Lambda_i = 0\} \times 1 \\
&\quad = 1 - \frac{\theta q}{\left(P_0/P_i^{\parallel}\right)(d_i/d)^{\alpha} + \theta}.
\end{aligned} \tag{14}$$

The generic second expectation term in (13) can be expressed, by using (8), in a similar way:

$$\begin{aligned}
&\mathbb{E}_{\{\mathbf{P}_j^{(\perp\to\parallel)}\},\{\Lambda'_j\}}\left[\exp\left(-\frac{\theta \mathbf{P}_j^{(\perp\to\parallel)}\left(d_j\right)\Lambda'_j}{P_0 L(d_0)}\right)\right] \\
&\quad = \mathbb{P}\left\{\Lambda'_j = 1\right\} \times \int_0^{\infty} \exp\left(-\frac{\theta p_j}{P_0 L(d_0)}\right) f_{\mathbf{P}_j^{(\perp\to\parallel)}}\left(p_j\right)\mathrm{d}p_j \\
&\qquad + \mathbb{P}\left\{\Lambda'_j = 0\right\} \times 1 \\
&\quad = 1 - \frac{\theta q}{\mathrm{XPD}_0 G(d, d_{\mathrm{ref}})\left(P_0/P_j^{\perp}\right)\left(d'_j/d_0\right)^{\alpha} + \theta}.
\end{aligned} \tag{15}$$

By plugging (14) and (15) into (13), one finally obtains expression (6) for the probability of successful transmission. □

Theorem 1 gives interesting insights on the expected performance in a dual-polarized transmission subject to background and internode interference. First, the leftmost term of the expression at the right-hand side of (6) is relevant in a situation where the throughput is limited by the

background (typically thermal) noise. In large and/or dense networks, the transmission is only limited by the interference and one can focus on the interference and polarization terms (i.e., the two other term of the expression, assuming N_0B is negligible). The first exponential term can be easily evaluated if $N_0B \neq 0$.

The second and the third terms of expression (6) relate to the interference generated by the surrounding nodes transmitting in co- and cross-polarized channels. These terms depend on (i) the polarization characteristics of the interfering nodes, (ii) the traffic statistics, and (iii) the topology of the network. Note that the impact of the topology has been largely investigated in [35] and we will limit our study to the effect of polarization.

Finally, channel correlation is neglected here, as often in the literature, for the purpose of analytical tractability and because these correlations do not change the scaling behavior of link-level performance. For the sake of completeness, we note that in [36] an analysis of the impact of channel correlation is carried out. The authors conclude that, when the traffic is limited ($q < 0.3$), the assumption of uncorrelation holds. On the other hand, when the traffic is intense ($q \geq 0.3$), the link probability of success is higher in the correlated channel scenario than in the uncorrelated channel scenario.

2.2. Probabilistic Link Throughput. Referring back to our definition of the probabilistic coexistence of the primary and secondary terminals in (1), a *transmission is said to be successful* if and only if the primary terminal is not in an outage for a fraction of time longer than $(1 - \varepsilon)$, that is, if the (instantaneous) SINR of the cognitive terminal is above the threshold θ. Therefore, we denote the probability of successful transmission in a primary link as $\mathcal{P}_s$, that is,

$$\mathcal{P}_s = \mathbb{P}\{\mathbf{SINR} > \theta\}. \tag{16}$$

The *probabilistic link throughput* [37] (adimensional) of a primary terminal is defined as follows:

(i) in the full-duplex communication case, it corresponds to the product of (a) $\mathcal{P}_s$ and (b) the probability that the transmitter actually transmits (i.e., q);

(ii) in the half-duplex communication case, it corresponds to the product of (a) $\mathcal{P}_s$, (b) the probability that the transmitter actually transmits (i.e., q), and (c) the probability that the receiver actually receives (i.e., $1 - q$).

The probabilistic link throughput can be interpreted as the unconditioned reception probability which can be achieved with a simple automatic-repeat-request (ARQ) scheme with error-free feedback [38]. For the slotted ALOHA transmission scheme under consideration, the probabilistic throughput in the half-duplex mode is then $\tau^{(\text{half})} \triangleq q(1 - q)\mathcal{P}_s$ and in full-duplex case $\tau^{(\text{full})} \triangleq q\mathcal{P}_s$.

2.3. Properties and Opportunities of Polarization Diversity. Theorem 1 expresses a network-wide condition to support the codeployment of primary and cognitive terminals. In order to implement polarization diversity and make it work, proper considerations have to be carried out. In this section, we propose several lemmas, all derived from Theorem 1, that allow to design and operate dual-polarized systems.

Lemma 2. *In a dual-polarized system subject to probabilistic coexistence of primary and secondary networks, relocating a cognitive terminal from the copolar channel to the cross-polar channel increases its probability of transmission while keeping intact the transmission capacity of the primary network.*

Proof. Let us consider a scenario with a single interferer located at distance d and transmitting with power P. For the ease of understanding, let us assume that if the terminal uses a polarized antenna, its probability of transmission will be denoted as $q = q^{\perp}$, whereas if a classical (not dual-polarized) scenario is considered, then $q = q^{\parallel}$.

If the cognitive terminal is using the copolar mode, the probabilistic coexistence condition (1) can be written as

$$\frac{\theta q^{\parallel}}{(P_0/P)(d/d_0)^{\alpha} + \theta} \leq \varepsilon; \tag{17}$$

whereas if the cognitive terminal is using the cross-polar mode, it holds that

$$\frac{\theta q^{\perp}}{\text{XPD}(d)(P_0/P)(d/d_0)^{\alpha} + \theta} \leq \varepsilon. \tag{18}$$

Therefore, the maximum acceptable probability of transmission in the copolar mode is

$$q^{\parallel}_{\max} = \varepsilon\left[1 + \frac{1}{\theta}\frac{P_0}{P}\left(\frac{d}{d_0}\right)^{\alpha}\right]. \tag{19}$$

Note that, on average, $\text{XPD}(d) \geq 1$ according to definition (8) and for physical reasons—the power leaked on the copolar dimension is *at most equal* to the power transmitted on the cross-polar channel. Finally, all other quantities in (19) are strictly positive and, therefore, one obtains that

$$q^{\parallel}_{\max} \leq \varepsilon\left[1 + \frac{\text{XPD}(d)}{\theta}\frac{P_0}{P}\left(\frac{d}{d_0}\right)^{\alpha}\right] = q^{\perp}_{\max}, \tag{20}$$

where the right-hand side expression for $q^{\perp}_{\max}$ derives directly from (18). Therefore, the thesis of the lemma holds. □

Lemma 2 indicates that polarization can be exploited as a diversity technique. Indeed, the achievable transmission rate will always be increased if the secondary network uses a polarization state that is orthogonal to that of the primary network and, furthermore, this remains true regardless of the values taken by the other system parameters (e.g., transmission power, acceptable outage rate ε, SINR value, etc.).

Lemma 3. *There exists a region of space, referred to as the primary exclusive region, where the cognitive terminals are not allowed to transmit and can be reduced by means of polarimetric diversity.*

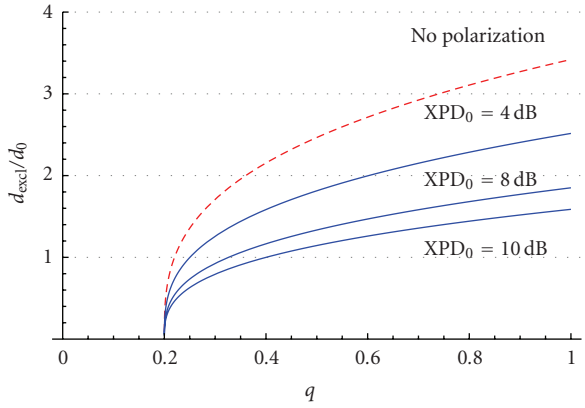

FIGURE 2: Primary exclusive region as a function of the terminal probability of transmission q, for various polarimetric values and with $\varepsilon = 0.2$.

Proof. As previously anticipated in Section 1, the primary exclusive region is completely characterized by the primary exclusive distance d_{excl}, that is, the minimum distance at which a cognitive terminal has to be, with respect to a primary receiver, so that it does not impact the capacity of the primary user (in a probabilistic sense) [21]. Starting from (6), in the presence of a single cross-polar interferer, one can write

$$\frac{\theta q}{\text{XPD}(d)(P_0/P)(d/d_0)^{\alpha} + \theta} \leq \varepsilon. \tag{21}$$

This relation is equivalent to

$$\frac{d}{d_0} \geq \left(\frac{1}{\text{XPD}_0 G(d, d_{\text{ref}})}\right)^{1/\alpha} \left(\theta \frac{P}{P_0} \frac{q-\varepsilon}{\varepsilon}\right)^{1/\alpha} \triangleq \frac{d_{\text{excl}}}{d_0}, \tag{22}$$

where the definition at the right-hand side allows to express the minimum distance d_{excl} as a function of the distance d_0 and the other main system parameters as follows:

$$d_{\text{excl}} = d_0 \left(\frac{1}{\text{XPD}_0 G(d, d_{\text{ref}})}\right)^{1/\alpha} \left(\theta \frac{P}{P_0} \frac{q-\varepsilon}{\varepsilon}\right)^{1/\alpha}. \tag{23}$$

Therefore, since $\alpha \geq 2$, using polarization diversity, that is, causing $\text{XPD}_0 G(d, d_{\text{ref}}) > 1$, reduces d_{excl}. □

In Figure 2, the normalized primary exclusive distance, defined as d_{excl}/d_0, is shown, as a function of the terminal probability of transmission q, with $\varepsilon = 0.2$. It can be observed that in the case without polarization, one always has $d_{\text{excl}} \gg d_0$, that is, the cognitive terminals must be located *outside* the transmission zone defined by the primary emitter-receiver distance. On the opposite, it is possible to operate a cognitive terminal inside this region (i.e., with $d_{\text{excl}} < d_0$) when the polarimetric dimension is used. Furthermore, in both cases the exclusive distance increases as a function of the terminal probability of transmission but its gradient is smaller in the dual-polarized case.

It is interesting to observe that relation (21) can also be used to parameterize practical realizations of the antennas. Indeed, it yields that

$$\text{XPD}(d) \geq \frac{P}{P_0} \left(\frac{d_0}{d}\right)^{\alpha} \frac{(q-\varepsilon)}{\varepsilon} \theta \tag{24}$$

from which, with $\text{XPD}(d) = \text{XPD}_0 G(d, d_{\text{ref}})$, it follows that

$$\text{XPD}_0 \geq \frac{1}{G(d, d_{\text{ref}})} \frac{P}{P_0} \left(\frac{d_0}{d}\right)^{\alpha} \frac{(q-\varepsilon)}{\varepsilon} \theta. \tag{25}$$

Therefore, the quantity at the right-hand side of (25) represents the minimum amount of XPD that the antenna of the cognitive terminal must possess. This value depends on the network configuration but also on the propagation environment (through the depolarization function $G(d, d_{\text{ref}})$).

Lemma 4. *If $q < \varepsilon$, polarization diversity is not required to achieve a probabilistic coexistence.*

Proof. As previously introduced, the coefficient XPD_0 is greater than or equal to 1. Therefore, the minimum value of XPD_0 to guarantee error-free transmissions on the cross-polar channel is

$$\text{XPD}_0 = \max\left\{1, \frac{1}{G(d, d_{\text{ref}})} \frac{P}{P_0} \left(\frac{d_0}{d}\right)^{\alpha} \frac{(q-\varepsilon)}{\varepsilon} \theta\right\}. \tag{26}$$

In (25), all quantities are greater than zero. Therefore, if $q < \varepsilon$, the quantity $q - \varepsilon$ is always negative and the solution of (26) is $\text{XPD}_0 = 1$. □

Lemma 4 indicates that, if the desired throughput remains limited, then the outage is guaranteed on the primary system without summoning up the diversity of polarization on the secondary terminal. Therefore, the cross-polar channel can be kept available for other terminals that may require higher data rates. This can be observed in Figure 2.

Theorem 5. *Besides being limited by probabilistic coexistence considerations, there exists an optimum probability of transmission by a terminal in the primary network, denoted as q_{opt}, that maximizes the throughput.*

Proof. Let us define the optimal user probability of transmission as

$$q_{\text{opt}} \triangleq \arg\max_{q} \tau, \tag{27}$$

where the probabilistic throughput τ has been defined in Section 2.2. We first focus on half-duplex systems, using polarization diversity: in this case, the link throughput is $\tau = q(1-q)\mathcal{P}_s$. Since $\ln(\cdot)$ is a monotonically increasing function, finding the maximum of τ is equivalent to finding the maximum of $\ln(\tau)$, that is,

$$q_{\text{opt}} = \arg\max_{q} \ln(\tau). \tag{28}$$

In order to find the maximum, we compute the partial derivative of $\ln(\tau)$ with respect to q:

$$\frac{\partial}{\partial q}\ln(\tau) = \frac{1}{q} - \frac{1}{1-q} + \frac{\partial}{\partial q}\sum_{j}^{N_{\text{int}}^{\perp}} \ln\left(1 - \frac{q}{\eta_j}\right), \tag{29}$$

where

$$\eta_j \triangleq \frac{\text{XPD}_0}{\theta} G(d, d_{\text{ref}}) \frac{P_0}{P_j^{\perp}} \left(\frac{d'_j}{d_0}\right)^{\alpha} + 1. \tag{30}$$

By using the approximation (This approximation is accurate for $0 < q < \eta_j/3$, which is always verified since d'_j and XPD_0 need to be kept high because of the probabilistic coexistence constraint.) $\ln(1+x) \approx x$ and setting $\partial \ln(\tau)/\partial q = 0$, one has

$$\left(q_{\text{opt}}\right)^2 - q_{\text{opt}}(1 + 2\eta) + \eta \approx 0, \tag{31}$$

where $\eta \triangleq 1/\sum_j^{N_{\text{int}}^{\perp}} \eta_j^{-1}$. The positive solution of this equation is given by

$$q_{\text{opt}} \approx \eta + \frac{1}{2}\left(1 - \sqrt{1 + 4\eta^2}\right) \tag{32}$$

which is the probability of transmission that maximizes the throughput. The same derivation can be applied in the case of a full duplex system and leads to the solution $q_{\text{opt}} \approx \eta$. If the approximation $\ln(1+x) \approx x$ is not used, then the optimal probability of transmission cannot be given in a closed-form expression but has to be numerically evaluated. □

Obviously, the maximum value of q will be the minimum between (i) the optimum probability of transmission in a slotted transmission system (in a general sense), given by (32), and (ii) the maximum rate that can be achieved under the constraint of a probabilistic coexistence in (20). Therefore, before selecting its transmission rate, a cognitive terminal must evaluate these two quantities, on the basis of the available information stored in the databases (positions of the nodes, acceptable outage, etc.), and use the smallest one.

In Figures 3(a) and 3(b), the accessible and optimal terminal probabilities of transmission are presented as functions of d/d_0, in the cases with (a) half duplex and (b) full duplex communications, respectively. In each case, two polarization strategies are considered: (i) no polarization and (ii) $\text{XPD}_0 = 10\,\text{dB}$. The accessible regions are defined by means of the inequality (22). In particular, the leftmost border of each exclusive region, denoted as line q_{excl}, is defined as the probability of transmission for a terminal at the boundary of the primary exclusive region, that is, with $d = d_{\text{excl}}$.

From these figures, it can be observed that the probability of transmission of dual-polarized cognitive systems is mainly limited by the interference bound imposed to protect the primary system. In fact, the transmission rate of the terminals will nearly always be lower than the optimal transmission rate, except when the cognitive terminal is distant. In that specific case, the optimum probability of transmission (20) in the accessible region (in a probabilistic sense) saturates, that is, it reaches $q_{\text{opt}} \approx 1/2$ in the half-duplex case and $q_{\text{opt}} \approx 1$ in the full-duplex case. Note that these values correspond to the maximum achievable throughput observed in any half-duplex or full-duplex system. Indeed, the definitions of the probabilistic link throughput are $\tau^{(\text{half})} \triangleq q(1-q)\mathcal{P}_s$ and $\tau^{(\text{full})} \triangleq q\mathcal{P}_s$ and the corresponding optimum terminal probabilities of transmission cannot exceed $q = 1/2$ and $q = 1$, respectively.

In the scenarios where polarimetric diversity is exploited, this crossover distance is smaller ($d_{\text{excl}}/d_0 \approx 1.5$) than in the classical case ($d_{\text{excl}}/d_0 \approx 3.3$). Comparing the results in Figure 3(a) with those in Figure 3(b), another observation can be carried out. In the half-duplex case, for each distance $d > d_{\text{excl}}$, the optimal transmission probability q_{opt} lies inside the accessible region. In other words, q has to be properly selected to maximize the throughput. In the full-duplex case, $q_{\text{opt}} \approx 1$ everywhere in the exclusive region. These observations will be confirmed by the results presented in Section 4.

Finally, it is confirmed that, in the accessible regions, one either has (i) $(d'_j/d_0)^{\alpha} \gg 1$ with $\text{XPD}_0 > 1$ (i.e., $q/\eta_j \ll 1$) or (ii) $q_{\text{opt}} \ll 0.3$. Therefore, the approximation used in proof of Theorem 5 (i.e., $\ln(1+x) \approx x$) holds and the value of q_{opt} derived in Theorem 5 can be considered as an accurate approximation of the true value.

2.4. Considerations for Practical System Implementation. In the previous subsections, we have shown that the capacity of a primary user can be guaranteed, while, at the same time, allowing efficient spectrum access, if the polarimetric dimension is exploited. Moreover, dual-polarized terminals will benefit from an increase of capacity by means of a higher transmission rate and reduced terminal-to-terminal interference. The efficiency of polarization diversity depends on the cross-polar discrimination of the antennas in use. More precisely, the value of the initial cross-polar discrimination (i.e., XPD_0) has to be as high as possible; yet, the XPD of well-designed antennas is typically on the order of $10 \div 20\,\text{dB}$ [15, 39], which allows a significant discrimination between copolar and cross-polar channels. Depending on the achievable value of XPD_0, the outage rate of a primary terminal, and the location of the terminals, the transmission rate of a cognitive terminal can be adapted taking into account the relations (20) and (32). Finally, the primary exclusive region can be determined by means of (22) and notified to the cognitive terminals which, in turn, can use it as a constraint.

3. Experimental Determination of the Indoor-to-Indoor and Outdoor-to-Indoor XPD

Several previous works have been undertaken in order to model the XPD for different kinds of environment. In [20], a theoretical analysis is conducted for the small-scale variation of XPD in an indoor-to-indoor scenario and it is concluded that it has a doubly, noncentral Fisher-Snedecor distribution.

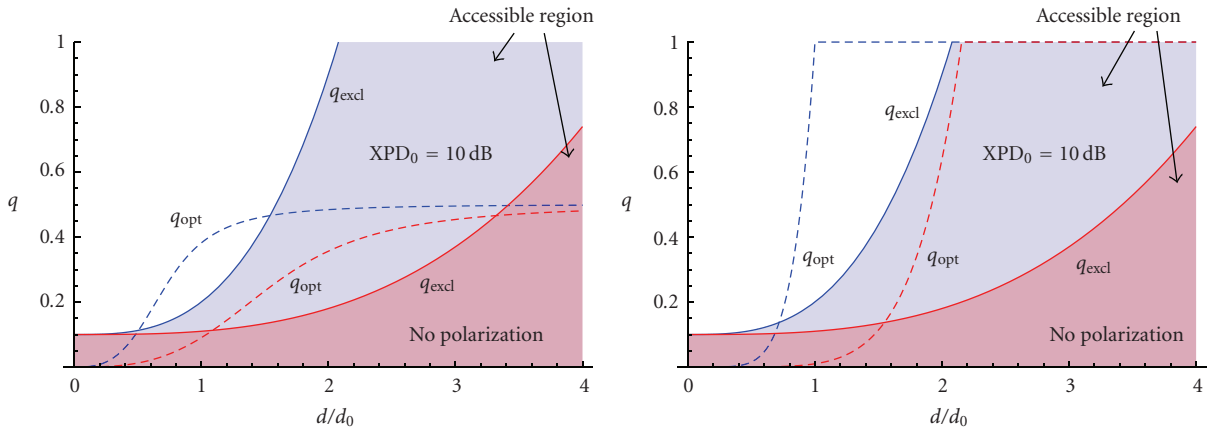

(a) Half duplex communications

(b) Full duplex communications

FIGURE 3: Accessible and optimal terminal probabilities of transmission as a function of d/d_0 and for $\varepsilon = 0.1$. In both cases, two polarization strategies are considered: (i) no polarization (drawn in red) and (ii) polarization with $XPD_0 = 10$ dB (drawn in blue).

A mean-fitting (i.e., the pathloss) model of XPD as a function of the distance in an outdoor-to-outdoor scenario was studied in [16, 19]. The corresponding performance is analyzed in [11].

In this paper, we provide the reader with original measurements campaigns in both indoor-to-indoor and outdoor-to-indoor scenarios. Indeed, these correspond to real-life situations where various technologies, such as WiFi, sensor networks, personal area networks (indoor-to-indoor scenarios) or WiMax, public WiFi, and 3G systems (outdoor-to-indoor scenarios) are in use.

We consider three generic models to describe the variation of the XPD with respect to the distance. For instance, when the transmission ranges are long (several hundreds of meters or a few kilometers), the best expression for the path loss function is

$$G_1(d, d_{\text{ref}}) = \left(\frac{d}{d_{\text{ref}}}\right)^{-\beta}, \tag{33}$$

where β is a decay factor ($0 < \beta \leq 1$). On the other hand, when distances are small (tens of meters) or in indoor-to-indoor scenarios, the XPD value, in decibels, decreases linearly with respect to the distance. In other words, one can write

$$\text{XPD}(d)\,[\text{dB}] = \text{XPD}_0\,[\text{dB}] - \gamma d \tag{34}$$

which corresponds, in linear scale, to the following path loss function:

$$G_2(d, d_{\text{ref}}) = 10^{-(\gamma/10)d}. \tag{35}$$

Finally, in some indoor scenarios where the transmission distances are small, it was observed that the XPD remains constant, that is,

$$G_3(d, d_{\text{ref}}) = 1. \tag{36}$$

In the remainder of this section, we characterize the applicability of the three XPD models just introduced. In other words, we consider an experimental setup and, on the basis of an extensive measurement campaign, we determine which XPD model is to be preferred in each scenario of interest (indoor-to-indoor and outdoor-to-indoor).

3.1. Setup. The measurements were performed using a Vector Signal Generator (Rohde & Schwarz SMATE200A VSG) at the transmitter (Tx) side and a Signal Analyzer (Rohde & Schwarz FSG SA) at the receiver (Rx) side. The Tx chain was composed of the VSG and a directional antenna. The Rx antenna was a tri-polarized antenna, made of three colocated perpendicular antennas. Two of these antennas were selected to create a Vertical-Horizontal dual-polarized antenna. The three receiver antennas were selected one after another by means of a switch and were connected to the Signal Analyzer through a 25 dB, low-noise amplifier. The Rx antennas were fixed on an automatic positioner to create a virtual planar array of antennas. A continuous wave (CW) signal at the frequency of 3.5 GHz was transmitted and the corresponding frequency response was recorded at the receiver side. The antenna input power was 19 dBm.

The measurement site was the third floor of a building located on the campus of Brussels University (ULB) and referred to as "Building U." In the outdoor-to-indoor case, shown in Figure 4(a), the transmitter was fixed on the rooftop of a neighboring building (referred to as "Building L"), at a height of 15 m and was directed toward the measurement site. A brick wall was separating the line-of-sight (LOS) direction between this measurement site and the transmitter. The measurements were performed in a total of 78 distinct locations and in seven successive rooms. The rooms were separated by brick walls and closed wooden doors. The distance between the transmitter and the measurement points was in the range between 30 m and 80 m. In the indoor-to-indoor case, shown in Figure 4(b), the Tx antenna was fixed in the first room and was directed toward the seven next rooms, in which 65 measurement points were considered. The distance between the transmitter

and the measurement points was in the range between 8 m and 55 m. In order to characterize the small-scale statistics of XPD a total of 64 spatially separated measurements were taken at each Rx position and in an 8×8 grid. The spacing between grid points was $\lambda/2 = 4$ cm. At each grid point, 5 snapshots of the received signal were sampled and averaged to increase the signal-to-noise-ratio.

3.2. Experimental Results and Their Interpretation. The analysis of the collected experimental results has shown that the values of the XPD, for a given distance, present a location-dependent variability. Therefore, in the following figures, where the XPD is shown as a function of the distance d, the average value is shown along with the 1σ and 2σ being confidence intervals. Since the spatial variations were found to be Gaussian, these intervals account for 68% and 95% of the observed sets, respectively.

The horizontal polarization was first used in an indoor-to-indoor scenario and is reported in Figure 5. It was observed that the XDP can be accurately modeled by means of the propagation model $G_2(d, d_{\text{ref}})$ where one has $\text{XPD}_0 = 11.3$ dB, $d_{\text{ref}} = 1$ m, and $\gamma = 0.16$ dB/m. The variation around the average value was also analyzed and the corresponding cumulative distribution function (CDF) is shown in Figure 6. This variation was found to fit with a zero-mean Gaussian random variable with standard deviation equal to 0.295 dB. It is interesting to note that, unlike the case of the outdoor-to-outdoor scenarios presented in [19], the behavior of the XDP depends on the initial polarization of the antenna. More precisely, the results in Figure 6 correspond to a horizontal polarization while the results in Figure 7 correspond to an initial vertical polarization. It can be seen that, in the latter scenario, the XPD is almost constant and equal to $\text{XPD}_0 = 4$ dB. In this case, the XPD variability can be modeled as a zero-mean Gaussian random variable with standard deviation equal to 2.75 dB.

Finally, the results collected in an outdoor-to-indoor scenario are presented in Figure 8. As expected, the XPD is a decreasing function of the distance and is suitably modeled by using the propagation model $G_2(d, d_{\text{ref}})$, with $\text{XPD}_0 = 12.87$ dB, $d_{\text{ref}} = 20$ m, and $\gamma = 0.13$ dB/m. The spatial variability can be modeled as a zero-mean Gaussian random variable with standard deviation equal to 2.95 dB. Note that full de-polarization occurs after a hundred of meters and the two initial polarizations (i.e., horizontal and vertical) lead to the same behaviour.

4. Numerical Performance Evaluation

In this section, a numerical analysis of the performance of the proposed dual-polarized cognitive systems is presented. In Section 3, it has been shown that the XPD experiences spatial shadowing: more precisely, at a fixed distance different values of the XPD can be observed at different locations. The system parameters for performance analysis are selected by taking into account this normal fluctuation. Therefore, instead of using the average value for XPD_0, it is preferable to use a value (denoted as $\text{XPD}_0^{\min}$) that can be observed with a confidence equal to a predefined value $\delta \in (0, 1)$. Taking into account that XPD_0 has a Gaussian distribution, it follows that

$$\mathbb{P}\left\{\text{XPD}_0 \leq \text{XPD}_0^{\min}\right\} = 1 - Q\left(\frac{\text{XPD}_0^{\min} - \mu}{\sigma}\right) = \delta, \quad (37)$$

where μ and σ are the average value and the standard deviation of the observed XPD_0, respectively. Therefore, $\text{XPD}_0^{\min}$ can be expressed as

$$\text{XPD}_0^{\min} = \mu + \sigma Q^{-1}(\delta). \quad (38)$$

For instance, if a confidence level of 80% is required (i.e., $\delta = 0.8$), one has to select $\text{XPD}_0^{\min} = \mu - \sigma Q^{-1}(0.8) \approx \mu - 0.81\sigma$. This approach will be used to set the initial parameters in the following performance analysis.

4.1. Full Duplex Systems in an Outdoor-to-Indoor Scenario. Cellular system typically corresponds to an outdoor-to-indoor scenario. Examples include WiMax base stations or cellular mobile phone systems. A typical scenario is presented in Figure 9. Referring to the experimental results presented in Section 3, we used in our simulations the model $G_1(d, d_{\text{ref}})$ with parameters $\alpha = 3$, $\beta = 0.4$, and $\text{XPD}_0 = 4 \div 10$ dB. Also, the measurements lead us to set $\text{XPD}_0^{\min}$ equal to 10.48 dB with an 80% confidence level. The cell radius is $r = 200$ m, 10 cognitive terminals are deployed, their distances uniformly distributed over $[0, r]$. Finally, the Tx-Rx distance in the primary network is $d_0 = 30$ m.

Two different polarization strategies are investigated: (i) the primary and the cognitive networks do not use polarimetric diversity (this scenario is referred to as *no polarization*) and (ii) the systems reduce their interference by using two orthogonal polarization states (this scenario is referred to as *full polarization*).

In Figure 11, the performance of full duplex systems is presented. More specifically, in Figure 11(a), the throughput of the system is shown as a function of the terminal probability of transmission. It can be seen that the throughput of the dual-polarized system is significantly higher, particularly when the probability of transmission is high. In Figure 11(b), the corresponding link probability of success in the primary network is investigated. It can be seen that it confirms the conclusions of Lemma 2: for a given minimum value of the link probability of success, the achievable transmission rate is significantly higher in the dual-polarized mode with respect to the value observed with the classical approach. For instance, with $\varepsilon = 0.8$, one has $q_{\max} = 0.15$ while, by using the dual-polarized approach, the maximum probability of transmission can be increased up to $q_{\max} = 1.0$. In other words, virtually any transmission rate is achievable with a limited impact on the primary system.

4.2. Half-Duplex System in an Indoor-to-Indoor Scenario. In a second scenario, the probabilistic coexistence is analyzed in the context of half-duplex systems, where indoor-to-indoor transmissions are typically used. Examples include wireless sensor networks (WSNs), ZigBee systems, and body area net-

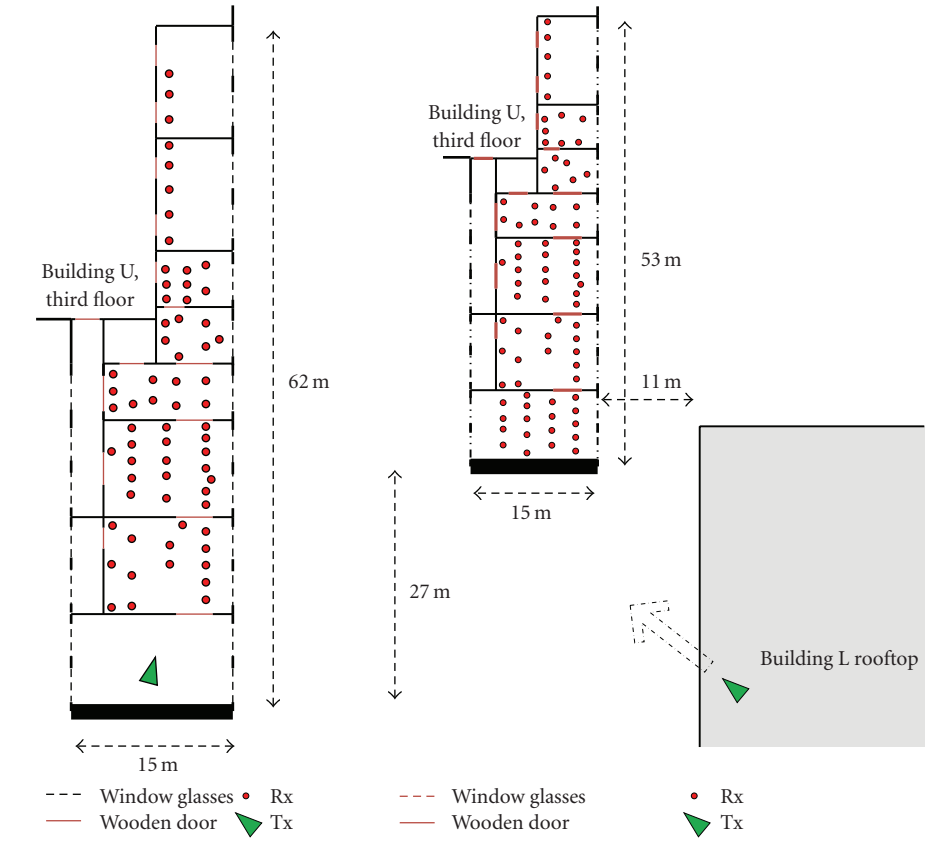

(a) Indoor-to-indoor measurement setup (b) Outdoor-to-indoor measurement setup

FIGURE 4: Scenario descriptions.

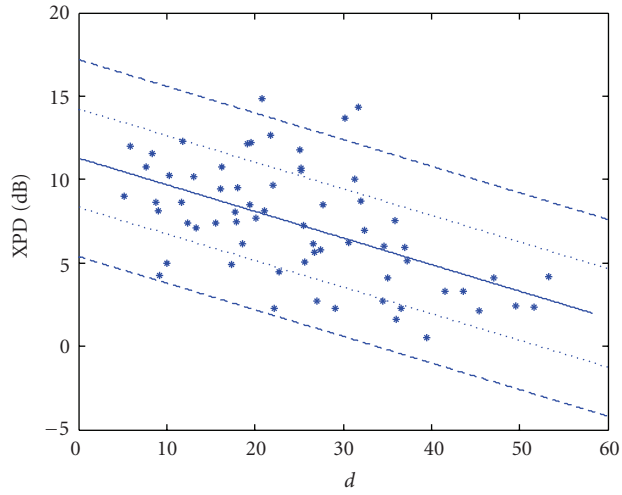

FIGURE 5: XPD in logarithmic scale, as a function of the Tx distance, in the indoor-to-indoor scenario with an initial horizontal polarization.

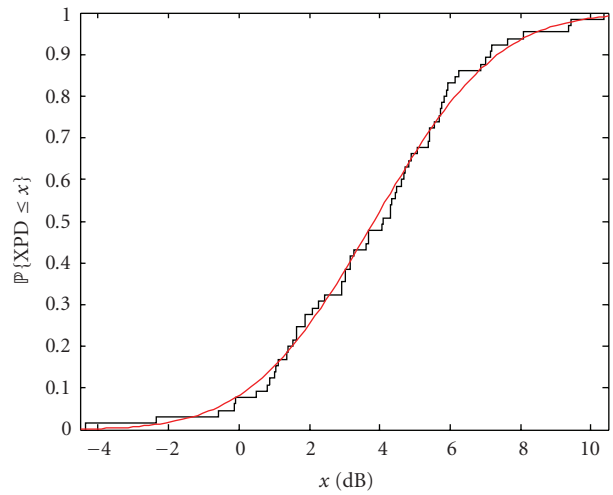

FIGURE 6: CDF of the XPD in the indoor-to-indoor scenario.

works (BANs). A typical scenario is presented in Figure 10. In our simulations, we considered a primary transmission at distance $d_0 = 15\,\text{m}$ and subject to interference from 5 terminals located at $d = 25\,\text{m}$ from the central base station. This corresponds to $d/d_0 \approx 1.67$ and it can be seen from Figure 3(a) that this value is in the accessible region. The propagation model $G_3(d, d_{\text{ref}})$ is used and the other relevant parameters are $\theta = 10\,\text{dB}$, $\text{XPD}_0 = 4$–$10\,\text{dB}$, and $\alpha = 3$.

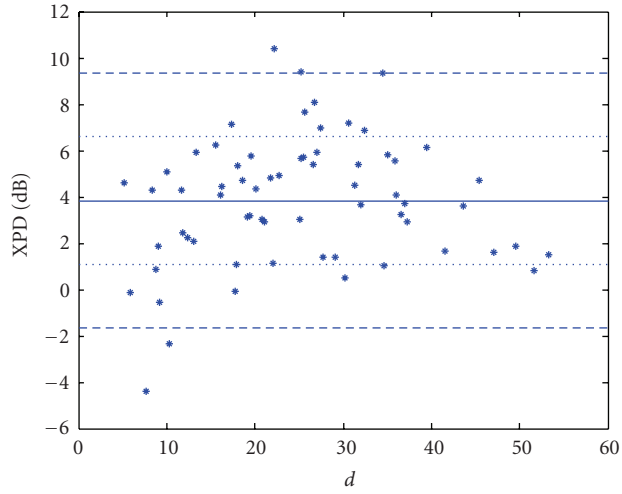

Figure 7: XPD in logarithmic scale, as a function of the Tx distance, in the indoor-to-indoor scenario with an initial vertical polarization.

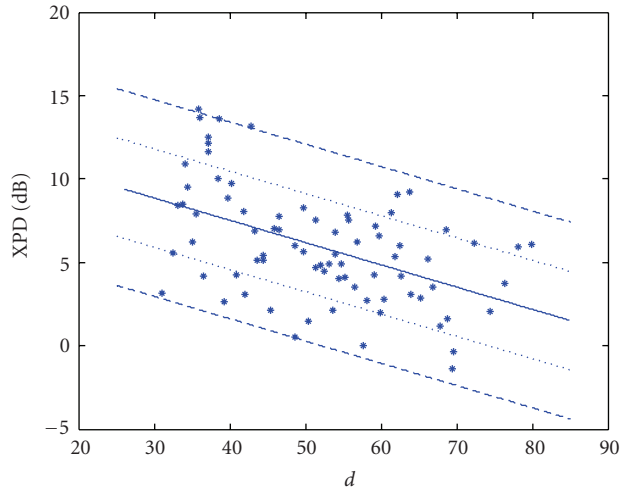

Figure 8: XPD (logarithmic scale) in the outdoor-to-indoor scenario.

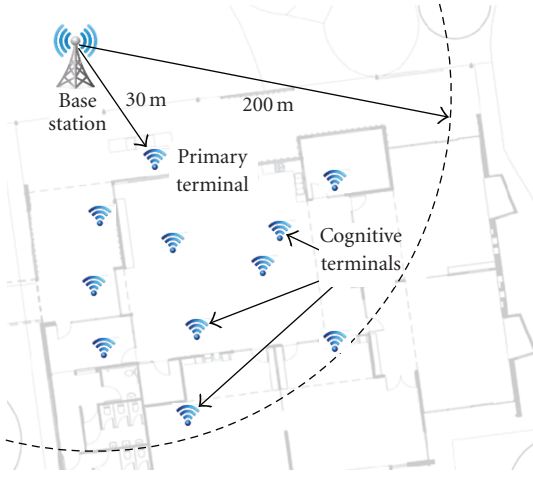

Figure 9: The outdoor-to-indoor scenario.

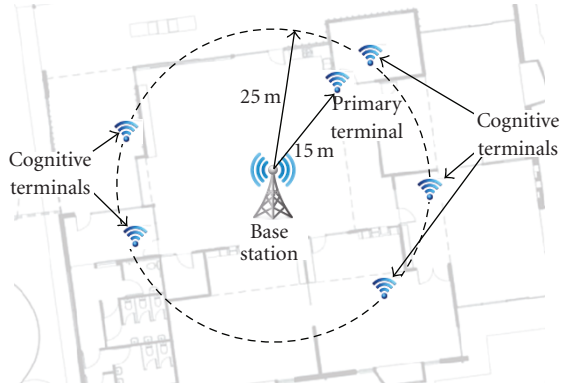

Figure 10: The indoor-to-indoor scenario.

The transmit power is the same at all nodes. Referring to the experimental analysis conducted in Section 3, one can observe that the values of interest for $\mathrm{XPD}_0^{\min}$ (with a 80% level of confidence) are 8.91 dB and 1.8 dB for horizontal and vertical polarizations, respectively.

In Figure 12, the performance of these half-duplex systems is presented. More particularly, in Figure 12(a), the throughput is shown as a function of transmission rate of the terminals, in a scenario with copolar interferers (i.e., without diversity of polarization) and under the dual-polarized scheme under study. It can be observed that the diversity of polarization drastically increases the throughput, even when the terminal probability of transmission is small. Regarding the probabilistic coexistence, in Figure 12(b) the link probability of success at the primary terminal is shown as a function of the transmission rate of the cognitive terminals. It can be observed that the use of polarization diversity gives a clear advantage in terms of interference limitation and available throughput for the cognitive terminals. For instance, with $\varepsilon = 0.8$ and a horizontal initial polarization, one has $q_{\max} = 0.07$ while, by using the dual-polarized approach, this quantity can be increased up to $q_{\max} = 0.25$ at each terminal. Finally, it can be seen that the optimum probability of transmission with XPD = 10 dB is approximately $q_{\mathrm{opt}} \approx 0.5$, which matches with the value of q_{opt} found in Figure 3(a).

5. Conclusions

In this paper, we have presented a novel theoretical framework to demonstrate the network-level performance increase that can be achieved in a polarimetric diversity-oriented system subject to Rayleigh fading and probabilistic coexistence of primary and secondary (cognitive) networks. The theoretical approach was supported by an extensive measurement campaign. It has been shown that different mathematical expressions must be used in order to suitably model the dependence of the XPD on the distance between transmitter and receiver. These models depend not only on the scenario of interest, but also on the initial antenna polarization. For instance, in an indoor-to-indoor scenario,

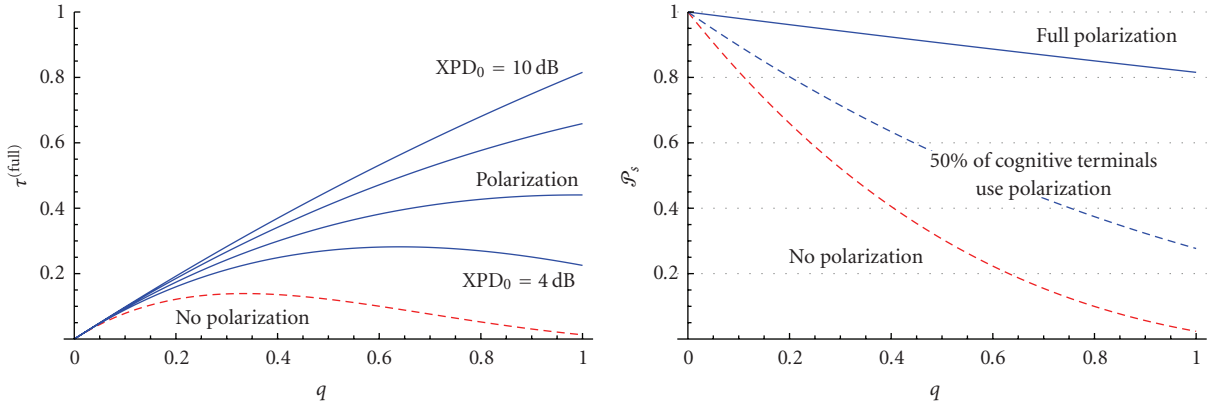

(a) Throughput as a function of the probability of transmission

(b) Link probability of outage on the primary network as a function of the probability of transmission

Figure 11: Performance analysis of a dual-polarized full-duplex cellular system.

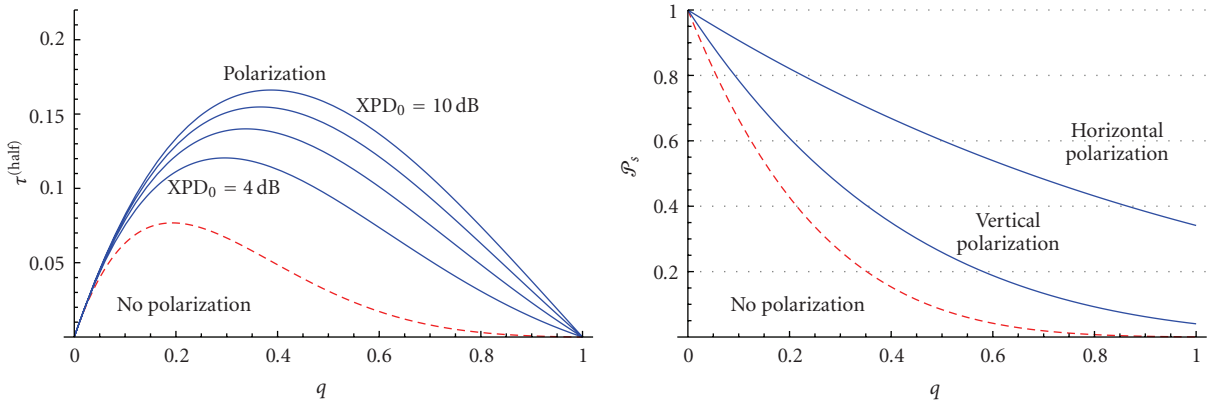

(a) Throughput as a function of the probability of transmission

(b) Link probability of outage on the primary network as a function of the probability of transmission

Figure 12: Performance analysis of a dual-polarized half-duplex system. The distance of the transmission is $d_0 = 15$ m and the 5 interferers are located at $d = 25$ m of the receiver.

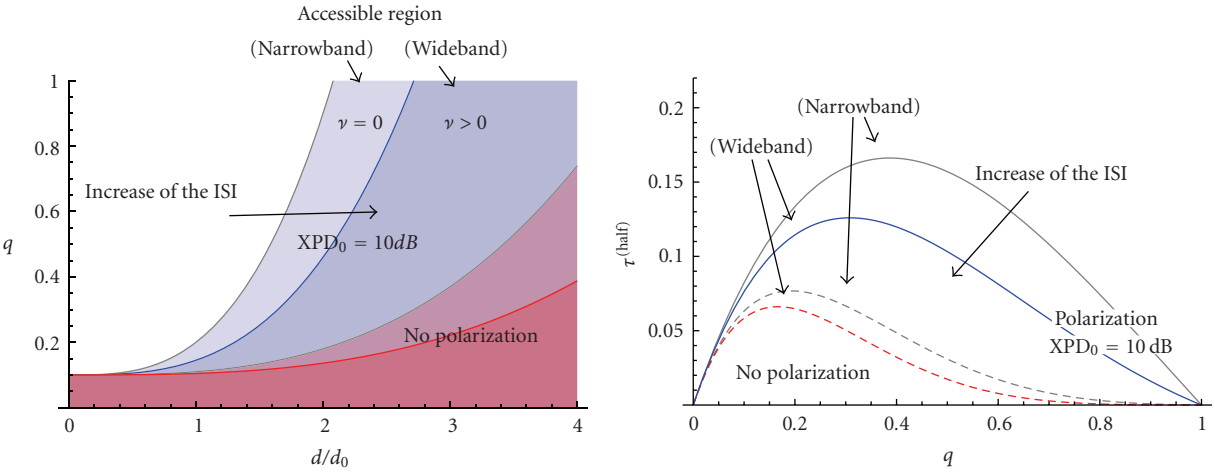

(a) Half duplex communications

(b) Throughput as a function of the probability of transmission

Figure 13: Impact of the channel fading on the system-level performance. The parameter value $\nu = 0$ and $\nu > 0$ correspond to narrowband scenarios and wideband scenario, respectively.

we have observed that the horizontal polarization provides a significant diversity (XPD_0 around 10 dB) while the vertical polarization leads to a more limited gain (XPD_0 around 4 dB).

Our results suggest that dual-polarized networks are of interest, even if orthogonality (indicated by the XPD value) is limited. Indeed, with respect to the classical implementation of probabilistic coexistence of primary and secondary networks on the same (single polarization) channel, the use of polarization diversity allows to remarkably increase the per-link throughput and reduce the primary exclusive region. In some cases (i.e., at low transmission rates), it could even be possible to deploy a cognitive terminal *closer* to a primary receiver than the primary transmitter itself, that is, inside the primary exclusive region.

Appendix

The performance analysis carried out throughout the paper applies to networking scenarios with narrowband fading. In this appendix, we present a preliminary, yet insightful, extension of our approach to encompass the presence of wideband fading.

In the presence of a transmission channel experiencing wideband fading, the transmitted symbols of the considered packet suffer from interference of the other symbols that have been delayed by multipath [33]. This phenomenon is referred to as Inter-Symbol-Interference (ISI) and it depends on the channel model, modulation format, and symbol sequence characteristics, among others [40–42]. Therefore, the expression of the ISI is hard to obtain and typically is not in closed form. In the network-level approach, we follow in this paper, an approximation to SINR in presence of wideband fading can be obtained by treating the ISI as an additive, uncorrelated, Rayleigh-faded noise power proportional to the received power [41]. The expression of the link-level SINR introduced in (5) becomes

$$\mathbf{SINR}_{\mathrm{wb}} \triangleq \frac{\mathbf{P}_0(d_0)}{N_0\mathrm{B} + \mathbf{P}_{\mathrm{int}} + \mathbf{P}_{\mathrm{ISI}}}, \tag{A.1}$$

where $\mathbf{P}_{\mathrm{ISI}}$ is noise power associated with the ISI. Its average value (noted $P_{\mathrm{ISI}} = \mathbb{E}[\mathbf{P}_{\mathrm{ISI}}]$) is supposed to be proportional to the received power [41] and can be defined as

$$P_{\mathrm{ISI}} \triangleq \nu P_0(d_0), \quad 0 \le \nu < 1. \tag{A.2}$$

Note that $\nu = 0$ refers to the narrowband scenario. Theorem 1 can now be extended to incorporate the case of wideband Rayleigh fading as follows. The probability that the SINR at the receiver exceeds a given value θ is

$$\begin{aligned}
&\mathbb{P}\{\mathbf{SINR}_{\mathrm{wb}} > \theta\} \\
&= \mathbb{E}[\mathbb{P}\{\mathbf{SINR}_{\mathrm{wb}} > \theta\} \mid \mathbf{P}_{\mathrm{int}}, \mathbf{P}_{\mathrm{ISI}}] \\
&= \mathbb{E}_{\mathbf{P}_{\mathrm{ISI}},\{\mathbf{P}_i^{\parallel}\},\{\Lambda_i\},\{\mathbf{P}_j^{(\perp\to\parallel)}\},\{\Lambda_j'\}} \\
&\quad \times \left[\exp\left(-\frac{\theta}{P_0 L(d_0)} \left(N_0 B + \sum_{i=1}^{N_{\mathrm{int}}^{\parallel}} \mathbf{P}_i^{\parallel} L(d_i)\Lambda_i \right.\right.\right. \\
&\qquad \left.\left.\left. + \sum_{j=1}^{N_{\mathrm{int}}^{\perp}} \mathbf{P}_j^{(\perp\to\parallel)} L\left(d_j\right)\Lambda_j' + \mathbf{P}_{\mathrm{ISI}} \right)\right)\right],
\end{aligned} \tag{A.3}$$

where the expectation of the term containing the ISI power becomes

$$\begin{aligned}
&\mathbb{E}_{\mathbf{P}_{\mathrm{ISI}},\{\mathbf{P}_i^{\parallel}\},\{\Lambda_i\},\{\mathbf{P}_j^{(\perp\to\parallel)}\},\{\Lambda_j'\}}\left[\exp\left(-\frac{\theta\mathbf{P}_{\mathrm{ISI}}}{P_0L(d_0)}\right)\right] \\
&\quad = \mathbb{E}_{\mathbf{P}_{\mathrm{ISI}}}\left[\exp\left(-\frac{\theta\mathbf{P}_{\mathrm{ISI}}}{P_0L(d_0)}\right)\right] \\
&\quad = \int_0^{\infty} \exp\left(-\frac{\theta x}{P_0L(d_0)}\right) f_{\mathbf{P}_{\mathrm{ISI}}}(x)\mathrm{d}x.
\end{aligned} \tag{A.4}$$

The definition of $\mathbf{P}_{\mathrm{ISI}}$ gives

$$f_{\mathbf{P}_{\mathrm{ISI}}}(x) = \frac{1}{P_{\mathrm{ISI}}} \exp\left\{-\frac{x}{P_{\mathrm{ISI}}}\right\} = \frac{1}{\nu P_0 L(d_0)} \exp\left\{-\frac{x}{\nu P_0 L(d_0)}\right\} \tag{A.5}$$

and, finally,

$$\mathbb{E}_{\mathbf{P}_{\mathrm{ISI}},\{\mathbf{P}_i^{\parallel}\},\{\Lambda_i\},\{\mathbf{P}_j^{(\perp\to\parallel)}\},\{\Lambda_j'\}}\left[\exp\left(-\frac{\theta\mathbf{P}_{\mathrm{ISI}}}{P_0L(d_0)}\right)\right] = \frac{1}{1+\nu\theta}. \tag{A.6}$$

Following the derivation outlined in the proof of Theorem 1, the link probability of successful transmission (A.3) in the wideband fading case finally becomes

$$\begin{aligned}
&\mathbb{P}\{\mathbf{SINR}_{\mathrm{wb}} > \theta\} \\
&\quad = \exp\left\{-\theta\frac{N_0B}{P_0d_0^{-\alpha}}\right\} \times \prod_{i=1}^{N_{\mathrm{int}}^{\parallel}} \left\{1 - \frac{\theta q}{\left(P_0/P_i^{\parallel}\right)(d_i/d_0)^{\alpha} + \theta}\right\} \\
&\qquad \times \prod_{j=1}^{N_{\mathrm{int}}^{\perp}} \left\{1 - \frac{\theta q}{\mathrm{XPD}_0 G(d, d_{\mathrm{ref}})\left(P_0/P_j^{\perp}\right)\left(d_j'/d_0\right)^{\alpha} + \theta}\right\} \\
&\qquad \times \left\{\frac{1}{1+\nu\theta}\right\}.
\end{aligned} \tag{A.7}$$

By comparing (A.7) with (6), it can be observed that the presence of wideband fading reduces the probability of successful link transmission by the factor $1/(1+\nu\theta)$. Since this factor is lower than 1 for $\nu \in (0;1]$, it can be concluded that the presence of ISI has a negative impact on the link probability of outage. Moreover, for a given value of ν, that

is, for a given level of ISI, the stronger this negative impact is, the higher is the considered SINR threshold θ. This, in turn, results in (i) an increase of the primary exclusive region (i.e., a reduction of the accessible region) and (ii) a degradation of system throughput. More precisely, in Figure 13(a) we clearly show the reduction of the comparison between the accessible transmission regions in the presence of narrowband fading (shown in Figure 3(a)) and in the presence of wideband fading (with $P_0/P_{\mathrm{ISI}} = 20\,\mathrm{dB}$). As one can see, the presence of a limited ISI has a detrimental impact, significantly increasing the primary exclusive region. In Figure 13(b), the throughput in the presence of ISI is shown in a scenario with half-duplex communications. In this case as well, the negative impact of wideband fading is evident.

Although the impact of frequency selective fading is detrimental, from these figures it can be concluded that, even in presence of wideband fading channel, the use of polarimetric diversity significantly increases the overall performance of the whole system and is thus of interest in the context of cognitive radio networks.

Acknowledgment

The support of the Belgian National Fund for Scientific Research (FRS-FNRS) is gratefully acknowledged.

References

[1] C. Cordeiro, K. Challapali, D. Birru, and S. Shankar, "IEEE 802.22: an introduction to the first wireless standard based on cognitive radios," *Journal of Communications*, vol. 1, no. 1, pp. 38–47, 2006.

[2] Q. H. Mahmoud, Ed., *Cognitive Networks*, John Wiley & Sons, New York, NY, USA, 2007.

[3] I. F. Akyildiz, W.-Y. Lee, M. C. Vuran, and S. Mohanty, "NeXt generation/dynamic spectrum access/cognitive radio wireless networks: a survey," *Computer Networks*, vol. 50, no. 13, pp. 2127–2159, 2006.

[4] F. K. Jondral, "Software-defined radio—basics and evolution to cognitive radio," *EURASIP Journal on Wireless Communications and Networking*, vol. 2005, no. 3, pp. 275–283, 2005.

[5] I. Budiarjo, M. K. Lakshmanan, and H. Nikookar, "Cognitive radio dynamic access techniques," *Wireless Personal Communications*, vol. 45, no. 3, pp. 293–324, 2008.

[6] R. Qingchun and L. Qilian, "Performance analysis of energy detection for cognitive radio wireless networks," in *Proceedings of the 2nd International Conference on Wireless Algorithms, Systems and Applications (WASA '07)*, pp. 139–146, Chicago, Ill, USA, August 2007.

[7] S. Xu, Z. Zhao, and J. Shang, "Spectrum sensing based on cyclostationarity," in *Proceedings of Workshop on Power Electronics and Intelligent Transportation System (PEITS '08)*, pp. 171–174, Guangzhou, China, August 2008.

[8] S. S. Barve, S. B. Deosarkar, and S. A. Bhople, "A cognitive approach to spectrum sensing in virtual unlicensed wireless network," in *Proceedings of International Conference on Advances in Computing, Communication and Control (ICAC '09)*, pp. 668–673, ACM, Mumbai, India, August 2009.

[9] FCC 08-260, "Second report and order and memorandum opinion and order," 2008, http://hraunfoss.fcc.gov/edocs_public/attachmatch/FCC-08-260A1.pdf.

[10] L. Berlemann and S. Mangold, *Cognitive Radio and Dynamic Spectrum Access*, John Wiley & Sons, New York, NY, USA, 2009.

[11] J.-M. Dricot, F. Horlin, and P. De Doncker, "On the coexistence of dual-polarized CDMA networks," in *Proceedings of the 4th International Conference on Cognitive Radio Oriented Wireless Networks and Communications (CROWNCOM '09)*, Hannover, Germany, June 2009.

[12] E. Baccarelli, M. Biagi, C. Pelizzoni, and N. Cordeschi, "Multi-antenna cognitive radio for broadband access in 4G-WLANs," in *Proceedings of the 5th ACM international Workshop on Mobility Management and Wireless Access*, pp. 66–73, ACM, Chania, Greece, October 2007.

[13] J.-A. Bazerque and G. B. Giannakis, "Distributed scheduling and resource allocation for cognitive OFDMA radios," *Mobile Networks and Applications*, vol. 13, no. 5, pp. 452–462, 2008.

[14] X. Wang and W. Xiang, "An OFDM-TDMA/SA MAC protocol with QoS constraints for broadband wireless LANs," *Wireless Networks*, vol. 12, no. 2, pp. 159–170, 2006.

[15] C. Oestges, "A comprehensive model of dual-polarized channels: from experimental observations to an analytical formulation," in *Proceedings of the 3rd International Conference on Communications and Networking in China (ChinaCom '08)*, pp. 1172–1176, Hangzhou, China, August 2008.

[16] M. Shafi, M. Zhang, A. L. Moustakas et al., "Polarized MIMO channels in 3-D: models, measurements and mutual information," *IEEE Journal on Selected Areas in Communications*, vol. 24, no. 3, pp. 514–526, 2006.

[17] F. Argenti, T. Bianchi, L. Mucchi, and L. S. Ronga, "Polarization diversity for multiband UWB systems," *Signal Processing*, vol. 86, no. 9, pp. 2208–2220, 2006.

[18] C. Oestges, V. Erceg, and A. J. Paulraj, "Propagation modeling of MIMO multipolarized fixed wireless channels," *IEEE Transactions on Vehicular Technology*, vol. 53, no. 3, pp. 644–654, 2004.

[19] V. Erceg, P. Soma, D. S. Baum, and S. Catreux, "Multiple-input multiple-output fixed wireless radio channel measurements and modeling using dual-polarized antennas at 2.5 GHz," *IEEE Transactions on Wireless Communications*, vol. 3, no. 6, pp. 2288–2298, 2004.

[20] F. Quitin, C. Oestges, F. Horlin, and P. De Doncker, "Small-scale variations of cross-polar discrimination in polarized MIMO systems," in *Proceedings of the 3rd European Conference on Antennas and Propagation (EuCAP '09)*, pp. 1011–1015, Berlin, Germany, March 2009.

[21] M. Vu, N. Devroye, and V. Tarokh, "On the primary exclusive region of cognitive networks," *IEEE Transactions on Wireless Communications*, vol. 8, no. 7, pp. 3380–3385, 2009.

[22] L. Giupponi and C. Ibars, "Distributed cooperation among cognitive radios with complete and incomplete information," *EURASIP Journal on Advances in Signal Processing*, vol. 2009, Article ID 905185, 13 pages, 2009.

[23] L. Le and E. Hossain, "Resource allocation for spectrum underlay in cognitive radio networks," *IEEE Transactions on Wireless Communications*, vol. 7, no. 12, pp. 5306–5315, 2008.

[24] N. Abramson, "The ALOHA system—another alternative for computer communications," in *Proceedings of Joint Computer Conference*, vol. 37 of *AFIPS Conference*, pp. 281–285, Houston, Tex, USA, November 1970.

[25] F. A. Tobagi, "Analysis of a two-hop centralized packet radio network—part I: slotted ALOHA," *IEEE Transactions on Communications Systems*, vol. 28, no. 2, pp. 196–207, 1980.

[26] D. Bertsekas and R. Gallager, *Data Networks*, Prentice-Hall, Upper Saddle River, NJ, USA, 2nd edition, 1992.

[27] R. Nelson and L. Kleinrock, "The spatial capacity of a slotted ALOHA multihop packet radio network with capture," *IEEE Transactions on Communications*, vol. 32, no. 6, pp. 684–694, 1984.

[28] H. Wu and Y. Pan, *Medium Access Control in Wireless Networks*, Nova Science, Hauppauge, NY, USA, 2008.

[29] Y. Kwon, Y. Fang, and H. Latchman, "Performance analysis for a new medium access control protocol in wireless LANs," *Wireless Networks*, vol. 10, no. 5, pp. 519–529, 2004.

[30] J. Weinmiller, M. Schläger, A. Festag, and A. Wolisz, "Performance study of access control in wireless LANs—IEEE 802.11 DFWMAC and ETSI RES 10 Hiperlan," *Mobile Networks and Applications*, vol. 2, no. 1, pp. 55–67, 1997.

[31] H.-Y. Hsieh and R. Sivakumar, "IEEE 802.11 over multihop wireless networks: problems and new perspectives," in *Proceedings of the 56th IEEE Vehicular Technology Conference (VTC '02)*, vol. 2, no. 2, pp. 748–752, Vancouver, Canada, September 2002.

[32] T. S. Rappaport, *Wireless Communications: Principles and Practice*, IEEE Press, Piscataway, NJ, USA, 1996.

[33] A. Goldsmith, *Wireless Communications*, Cambridge University Press, New York, NY, USA, 2005.

[34] J. A. Silvester and L. Kleinrock, "On the capacity of multihop slotted ALOHA networks with regular structure," *IEEE Transactions on Communications*, vol. 31, no. 8, pp. 974–982, 1983.

[35] O. Dousse, F. Baccelli, and P. Thiran, "Impact of interferences on connectivity in ad hoc networks," *IEEE/ACM Transactions on Networking*, vol. 13, no. 2, pp. 425–436, 2005.

[36] R. K. Ganti and M. Haenggi, "Spatial and temporal correlation of the interference in ALOHA ad hoc networks," *IEEE Communications Letters*, vol. 13, no. 9, pp. 631–633, 2009.

[37] M. Haenggi, "Outage, local throughput, and capacity of random wireless networks," *IEEE Transactions on Wireless Communications*, vol. 8, no. 8, pp. 4350–4359, 2009.

[38] S. Ahmed and M. S. Alam, "Performance evaluation of important ad hoc network protocols," *EURASIP Journal on Wireless Communications and Networking*, vol. 2006, Article ID 78645, 11 pages, 2006.

[39] C. A. Balanis, *Antenna Theory: Analysis and Design*, JWiley-Interscience, New York, NY, USA, 2005.

[40] J. C.-I. Chuang, "The effects of time delay spread on portable radio communications channels with digital modulation," *IEEE Journal on Selected Areas in Communications*, vol. 5, no. 5, pp. 879–889, 1987.

[41] S. Gurunathan and K. Feher, "Multipath simulation models for mobile radio channels," in *Proceedings of the 42nd IEEE Vehicular Technology Conference (VTC '92)*, pp. 131–134, May 1992.

[42] V. Fung, T. S. Rappaport, and B. Thomas, "Bit error simulation for pi/4DQPSK mobile radio communications using two-ray and measurement-based impulse response models," *IEEE Journal on Selected Areas in Communications*, vol. 11, no. 3, pp. 393–405, 1993.